Development of the BOLT II Roughness Experiment for Flight

Scott A. Berry[1]
NASA Langley Research Center, Hampton, Virginia, 23681

Michael T. Semper[2]
U.S. Air Force Academy, Colorado Springs, Colorado, 80840

Andrew K. Riha[3], C. Daniel Mullen[4], and Helen L. Reed[5]
Texas A&M University, College Station, Texas, 77843

Aaron T. Dufrene[6]
CUBRC Inc., Buffalo, New York 14225

Hermann F. Fasel[7]
University of Arizona, Tucson, AZ 85719

BOLT II is a sounding rocket research project with the goal of studying hypersonic boundary layer transition and turbulence. The BOLT II research vehicle is based on a three-dimensional geometry (a slightly longer version of BOLT) with concave surfaces and swept leading edges that provides two separate and distinct, also redundant, flow paths for conducting measurements. One side of BOLT II is dedicated to smooth surface transition and turbulence, to better study the natural instability processes, while the other has been assigned to study forced transition and turbulence using discrete roughness trips. The present paper is intended to document the primary drivers and decisions made leading up to finalizing the roughness side experiment for the BOLT II flight.

I. Nomenclature

M	=	Mach number
Re	=	unit Reynolds number (1/m)
$p_T'/\bar{p}_T$	=	freestream turbulence
k	=	boundary layer trip height (m)
b	=	boundary layer trip width (m)
δ	=	boundary layer thickness (m)
X	=	axial length (m)
Z	=	spanwise distance (m)

[1] Research Engineer, Aerothermodynamics Branch, M/S 408A, Associate Fellow AIAA.
[2] Researcher, Department of Aeronautical Engineering, AIAA Member.
[3] Ph.D. Student, Department of Aerospace Engineering, Student Member AIAA.
[4] Ph.D. Candidate, Department of Aerospace Engineering, Student Member AIAA.
[5] University Distinguished Professor, Department of Aerospace Engineering, Fellow AIAA.
[6] Aerospace Engineer, Aerothermal/Aero-Optics Evaluation Center, Senior Member AIAA.
[7] Professor, Department of Aerospace & Mechanical Engineering, Fellow AIAA.

II. Introduction

An ongoing series of sounding rocket flight experiments have been underway for more than a decade, first starting with the HIFiRE (Hypersonic International Flight Research and Experimentation) flights[1] and now the follow up BOLT (an acronym for **Bo**undary **L**ayer **T**ransition) flights.[2] BOLT is sponsored by the Air Force Research Laboratory (AFRL) and Air Force Office of Scientific Research (AFOSR) to study hypersonic boundary layer transition on increasingly complex configurations. While most of the HIFiRE flights were conducted on simple shapes, such as straight or elliptic cones, the BOLT vehicle was intended to represent a more realistic configuration (somewhat like a "waverider") with concave surfaces and swept leading edges. The expectation is that BOLT would stress our capability to analyze the boundary layer breakdown process, with multiple instability modes interacting and competing with each other leading to transition. There are two BOLT missions funded for flight: BOLT, with John Hopkins University Applied Physics Laboratory (JHU/APL) as the prime contractor, was recently launched this past summer (2021) out of Esrange in Sweden, and BOLT II, with Texas A&M and CUBRC as the lead, is now planning for a spring of 2022 launch, out of the NASA Wallops Flight Facility (WFF) in Virginia. Analysis of the BOLT flight is presently underway, some details from this first flight are to be discussed in Ref. 3.

The BOLT geometry, shown in Fig. 1, provides a low-curvature concave surface with swept leading edges that is indicative of a more realistic future hypersonic configuration, including pressure gradients and wall temperature effects. Computations to date have revealed a complex flow path that includes a center region whose boundary layer is relatively thick and stable, while the outer sections exhibit a much thinner boundary layer with a mixture of instability modes. BOLT II provides an opportunity to compare trips under a variety of boundary layer conditions. The basic research objective of the Side B roughness experiment is to improve knowledge regarding forced boundary layer transition and turbulence on a complex hypersonic vehicle. A sounding rocket flight test program provides the means to study forced transition and turbulence in low disturbance environments that typically cannot be obtained in ground-based facilities. Conventional facilities can provide the proper freestream conditions, but with added noise (disturbances that alter the boundary layer instabilities), while quiet facilities can provide less noise but not at matching freestream conditions to flight. For the BOLT II roughness experiment, a combined experimental & computational effort was established to inform decisions for placing and sizing the trips and laying out the sensor suite for flight. A wind tunnel test campaign was undertaken at the United States Air Force Academy's (USAFA) Mach 6 Ludwieg tube (M6LT), as replacement for the NASA LaRC 20" Mach 6 Tunnel (which was unavailable during the early stages of the COVID-19 pandemic). Computational mean flow solutions at wind tunnel and flight conditions were completed by Texas A&M to track streamlines for sensor placement and boundary layer information for scaling to flight.

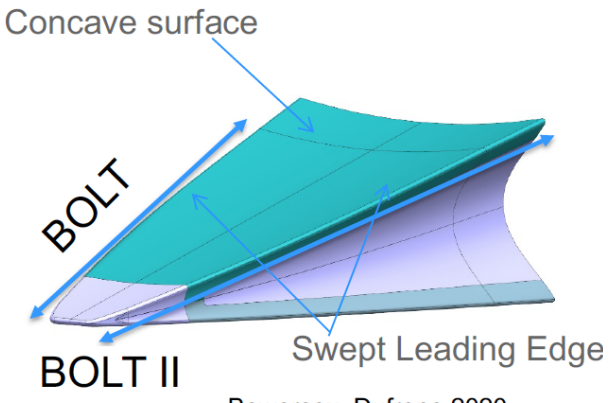

Figure 1. Sketch of BOLT vs. BOLT II.

While AFRL/AFOSR has primarily sponsored the BOLT flights as university-led projects to foster the next generation of researchers in hypersonic boundary layer transition and turbulence, NASA has also been involved with both campaigns as a contributing partner with support from the Hypersonic Technologies Project (HTP). At the NASA Langley Research Center (LaRC), the initial set of wind tunnel aeroheating data was obtained on the BOLT geometry and presented at the kick-off meeting, providing an early assessment of the transition fronts and behavior. These data, along with subsequent data obtained in other tunnels (including quiet facilities),[4] provided benchmark information for the many computations that were being done by the broader team (for example, see Refs. 5, 6 and 7). More recently, LaRC was tasked with leading the definition of the roughness experiments for the secondary side of both missions. Reference 8 provides an overview of the decisions that were made in defining the roughness side for the BOLT flight, which focused on the effect of steps on boundary layer transition at hypersonic conditions. For various reasons (to be discussed in detail in subsequent sections of the present paper), the roughness side for the BOLT II mission focused instead on discrete roughness effects. Presently, there are a number of research activities underway at LaRC to provide more insight into the various mechanisms at play in support of both missions, including computational efforts (for instance see Refs. 9 and 10). The purpose of the present paper, therefore, is to document decisions made in developing the roughness side experiment for the BOLT II flight.

BOLT vs. BOLT II

The intent of both BOLT flights is to provide high-quality flight data at hypersonic speeds of boundary layer instability mechanisms and the breakdown process to turbulence. As shown in Fig. 1, both use the same basic geometry, as the concave surfaces and swept leading edges are identical. BOLT is focused on measuring the instability modes ahead of transition, while BOLT II has an additional interest in seeing the resulting turbulent behavior and thus is a bit longer to increase the running length Reynolds numbers during flight (0.86 m for BOLT and 1.0 m for BOLT II). One side of both flight vehicles is dedicated to smooth surface transition (the primary focus of these flights), while the other (largely redundant) side is being utilized for conducting "roughness" experiments. As mentioned previously, NASA LaRC was tasked with providing leadership with deriving the roughness plans for both missions.

During the early design process for BOLT, concern was raised that the flight vehicle would have to be designed with different material at the nose, which then necessitated joint steps along the body. This led to some open questions about the joint steps and what effect they might have on the smooth side data. For this reason, the roughness experiment for BOLT was driven specifically to help answer the question about just how sensitive is the boundary layer to quasi "two-dimensional" steps spanning across the body. Surprisingly, not a lot of previous wind tunnel data and/or reports were found that could provide insight into the effect of steps (forward or rearward facing) on boundary layer transition at hypersonic flight conditions. Thus, the BOLT roughness experiment was designed, based on targeted and preliminary (and also somewhat limited) wind tunnel data, to study the effect of exaggerated joint steps (roughly three times larger than on the smooth side) on boundary layer transition. See Ref. 8 for more details about the roughness flight experiment for BOLT.

On the other hand, the flight hardware for BOLT II was redesigned[11] based on an updated trajectory (due to the use of a different launch vehicle stack) allowing different materials to be considered for the nose, which greatly reduced the likelihood and concern of joint steps for the second flight. This allowed the roughness experiment for BOLT II to be refocused on discrete roughness elements that have a recent wind tunnel pedigree, such as the diamond or "pizza box" trips. The goal, therefore, with BOLT II is to provide flight verification of discrete roughness correlations, such as the approach adopted for the Space Shuttle Orbiters that was developed based on extensive testing on moderately blunt configurations (such as the Orbiter or X-33 and X-38) at large angles of attack (~40-deg).[12] The key question for BOLT II is just how applicable is the Orbiter correlation for slender configurations (sharp nose vehicles at low angles of attack). Although it was not the intent going in, BOLT II could end up providing some of the "Orbiter-relevant" tripping data on slender configurations in flight that was sought during the failed HyBoLT (Hypersonic Boundary Layer Transition) mission in 2008 (see Ref. 13).

III. BOLT II Flight Analysis

As discussed in Ref. 11, BOLT II will fly on a two-stage sounding rocket from the NASA WFF, near Chincoteague, VA. The sounding rocket launch vehicle is comprised of a Terrier Mk. 70 first stage, followed by an Improved Malemute second stage. This two-stage system will provide exoatmospheric apogee and two test windows, one during ascent and the other during descent. The experimental payload includes the BOLT II flight geometry, the fairing (which transforms from the 3D shape to the conical section) and a transition module that houses most of the data acquisition and telemetry systems. During the test windows, Mach numbers greater than 5 and Reynolds numbers based on vehicle length between 1 and 35 million will be obtained. Figure 2 provides the ascent and descent trajectories during the test windows, and also identifies the eight trajectory points (x) used for the preliminary analysis of boundary layer properties, as well as the one (◊) used for the final design (to be discussed in the following sections). As mentioned previously, the flight vehicle was redesigned for this mission and includes a nickel 201 nose, stainless steel 401 body and aft attachment bulkhead. The vehicle also includes an internal class 4 tungsten ballast mass near the nose for enhanced aerodynamic stability. As with all spin-stabilized sounding rocket flights, the angle of attack is likely to vary some during flight. For the present analysis, the nominal angle of attack and yaw is zero. But actual flight values on the order of 2 deg or less are desired, while even up to 4 deg would be acceptable.

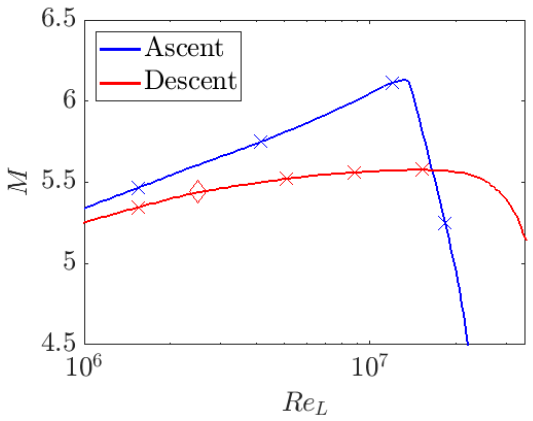

Figure 2. BOLT II test windows ascent and descent trajectories for identifying trajectory points for analysis.

IV. Preliminary Tripping Study at USAFA

An experimental study of the effect of boundary layer trip size (both height and width) and location was undertaken in the USAFA M6LT on a 33% scaled BOLT II flight test model. Freestream conditions in the tunnel were chosen to span the range expected during the upcoming BOLT II sounding rocket flight. Boundary layer trips were evaluated at multiple spanwise and streamwise locations on the BOLT II surface and included evaluations of combinations of trips as possible candidates for the final arrangement of trips to be used during the BOLT II flight test. In a separate follow up entry, the actual flight configuration was eventually tested at a range of conditions to provide comparison data to other ground tests and the eventual flight test results.

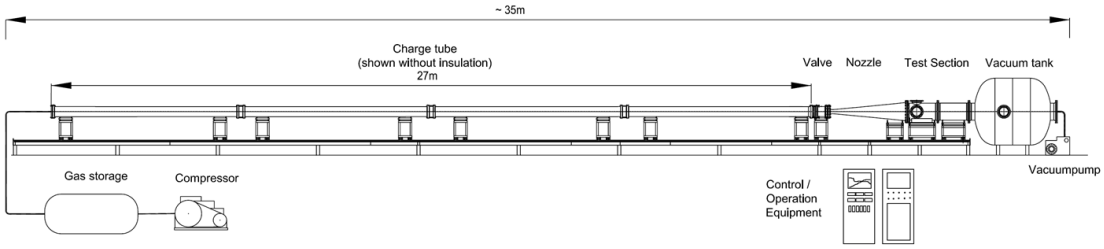

Figure 3. USAFA Mach 6 Ludwieg tube schematic.

A. Facility, Trip Design, & Experimental Setup

The USAFA M6LT was utilized for the present wind tunnel experiments. This relatively new facility was established at the USAFA in 2012 as a "conventional type" (meaning not a quiet tunnel) Ludwieg tube (see Ref. 14). A schematic of the tube is shown in Fig. 3 and Table 1 lists the important flow characteristics of the facility.

Table 1 USAFA Mach 6 Ludwieg tube characteristics.

Mach number	M = 5.9
Freestream turbulence	$p_T'/\bar{p}_T$ = 2 – 3%
Test gas	Air, dry
Temperature	Up to 673 K (500 K normal)
Unit Reynolds number range	Re = 2.5 – 30 x 10^6 m^{-1}
Run time	100 – 150 ms
Test section size	0.5 m diameter

USAFA designed and built the model and mounting strategy used for these experiments, and the model was fabricated using a ProJet 7000 3D printer with Accura Xtreme resin. The model dimensions were scaled to 33% of the flight vehicle size, to better fit within the test core of the M6LT. For mounting purposes, only the top half of the model was printed, giving a flat surface on the underside. Full information on the model including scaled dimensions and thermal properties of the model material can be found in Ref. 15. To avoid the upstream fast-acting valve wake on the tunnel centerline, the model was mounted on its side approximately 75 mm off centerline as shown in Fig. 4 and was viewed through a 200 mm sapphire window (mounted on the side of the tunnel opposite of the model).

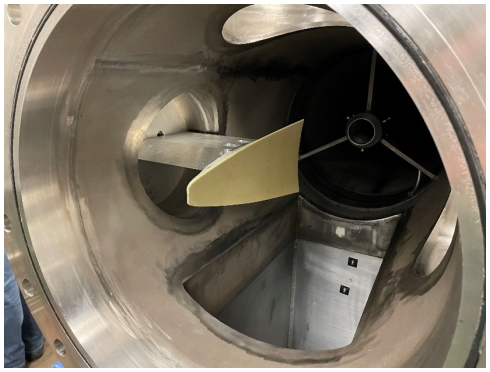

Figure 4. BOLT II model mounted in USAFA M6LT test section.

Temperature measurements on the surface of the model were made using a FLIR SC8303 infrared camera with a sensor size of 1,344 by 784 pixels and a framerate of 120 frames per second for this experiment. The selected calibration was from 10-90°C with a 1.95 ms integration time. Each run resulted in 10-12 frames of temperature data that were then exported and converted to heat flux following the methods of Ref. 16. Here, the surface is modeled as a semi-infinite flat plate, and heat conduction is governed by the classical heat conduction equation and boundary conditions. See Ref. 15 for a more detailed discussion of approach utilized to convert temperature data to heat flux, and then to the nondimensional Stanton number based on the computed flow properties and model wall temperature. A full list of tunnel flow conditions can also be found in Ref. 15.

Previous work (see Ref. 17) has been done on identifying successful trip geometries, and a key finding from previous research was that isolated trips, such as 3D vortex generating elements, were quite effective at promoting transition on bodies in hypersonic flows. Several different geometries were studied as discrete trip elements arranged in an array in front of the inlet to the Hyper-X hypersonic flight vehicle. Of the tested geometries, one of the better boundary-layer trips, and indeed one easily employed in hypersonic wind tunnel studies, is sometimes referred to as the "pizza box" trip (due to its stubby square shape), which is illustrated below in Fig. 5. This geometry is also often called the diamond trip, as the diagonal of the square is aligned with the oncoming flow (and thus resembles more of a diamond instead of a square). As the flow passes over the swept front face of the diamond trip and continues behind it, pairs of counterrotating vortices are created. These vortices propagate downstream and bring higher momentum fluid from the freestream and outer boundary layer down to the surface. Eventually, the entrainment of this high momentum fluid downward leads to increased instability which causes the boundary layer to eventually become turbulent. Due to the ease at which this type of trip can be added to subscale models tested in hypersonic wind tunnels using carefully cut and sized "stick-on" tape has led to it being used over the past couple of decades for numerous boundary layer trips studies, such as with the Space Shuttle, X-33, X-38, and others [for example, see Ref. 18]. This same approach was initially adopted for the present USAFA effort.

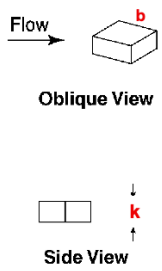

Figure 5. Pizza box trip geometry [17].

To aid in the spatial calibration and vortex tracking, fiducial markings were applied to the model surface. These fiducials are small painted dots using gold paint (the reflective nature of the gold allows for it to be easily seen in the infrared images) applied with the aid of a CNC machine for increased marking accuracy. The markings were made just large enough to show up on the infrared camera, but not so large as to induce flow disturbances themselves (as will be later proven from the baseline studies without trips). The schematic in Figure 6 shows the initial layout of the fiducial markings for the first round of experiments, and their locations relative to the leading edge of the model. Dots 1-8 mark the model centerline, while the uniform spanwise spacing of 10.1 mm represent possible locations for placement of trips (with heavy emphasis placed on the first three rows of fiducials, marked as Stations 1, 2, and 3 in Fig. 6). The red frame shown in the figure identifies the field of view obtained with the camera lens that was utilized for this study.

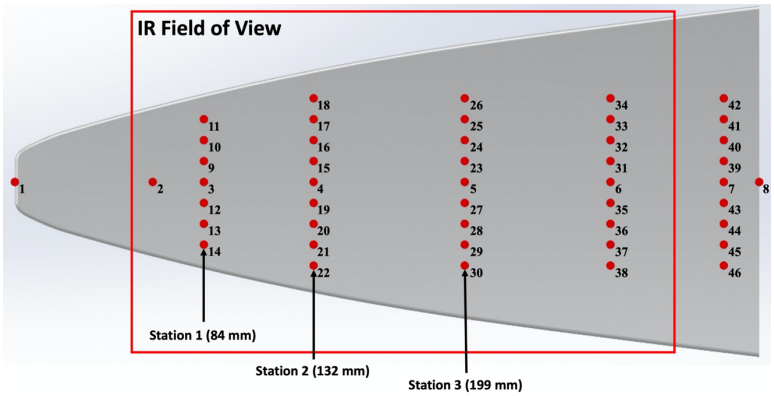

Figure 6. Initial set of model fiducials, station locations and field of view.

B. Initial Sizing Results

Normally the geometry of these trips (diagonal length, spacing, and height) is scaled to the local laminar boundary layer height, however, as this was a parametric study (and because boundary layer calculations were not available until the final selection process), a variety of trip dimensions were tested, as shown in Ref. 15. All the trips have a square planform, and the dimension listed in Table 2 is the side of the square, not the diagonal length. The trips with the four smallest heights (shown in bold font) in Table 2 were made from Teflon PTFE tape with adhesive that was applied directly to the model surface. The two larger trips of 2.5 and 3.7 mm heights were SLA printed and glued to the surface. The trips were applied just behind the fiducial markings, and a sample image showing an array of trips applied to the model surface is shown in Fig. 7. The thickness of the Teflon PTFE tape includes the adhesive layer, while the larger ones only reflect the thickness of the material used (however, the glue is not expected to add more than a small fraction to the overall height of the as-placed trip).

Table 2 Trip Dimensions.

Initial trip lengths, side (mm)	0.51, 1.0, 1.3, and 2.5
Initial trip heights (mm)	**0.29, 0.56, 0.81, 1.6**, 2.5, and 3.7

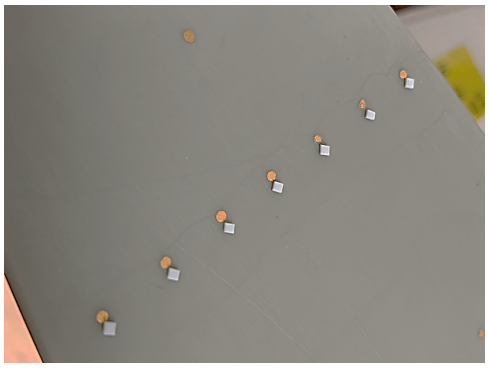

Figure 7. Trips applied to model; 0.56 mm height (and 1.3 mm width) trips shown.

Several series of runs were conducted using the fiducial layout of Fig. 6 above while altering trip height, location, and even planform dimensions. Baseline cases without trips were also recorded to compare the effect of the trips against the normal heating profile, although these results are more prominent in the later results as a background subtracted technique was utilized to visualize the effects of the trips more clearly after the initial parametric study. The first study involved placing a row of seven identical trips at the Station 1 location, completing runs between unit Reynolds numbers of 5-10 million/m, and then replacing the trips with increasingly taller ones as detailed in the first four values in Table 2. Unit Reynolds numbers above 10 million/m were initially tested, but due to the freestream fluctuations in the Ludwieg tube, much of the flow on the model became turbulent after this point. As the point of this study was to determine the effects of trips on a laminar boundary layer, the higher unit Reynolds number results were not pursued further. Some of the most relevant results are shown below in a grid array in Figure 8.

Starting with the first vertical column of results of Fig. 8 which provides the effect of no trips on the model surface and thus the baseline heating profile for the BOLT II geometry. The large dark (low heating) region of the model

centerline indicates a laminar boundary layer, even at the highest unit Reynolds number of 10 million/m. The boundary layer along the model centerline is also considerably thicker than at the outboard edges (based on the many calculations in the many references). The other largely prominent features on the surface are the two lobes of higher heating on the outboard edges of the model. Here, the swept edges induce crossflow, which trigger a much earlier transition of the boundary layer than on the centerline. These lobes grow in both heat flux intensity and size as the unit Reynolds number is increased, eventually almost reaching the Station 1 location where the trips are later applied. The boundary layer near the leading edges of the model is also thinner than on the centerline. Of important note, these lobes are not expected to appear at such low unit Reynolds numbers in flight. The noisy nature of a conventional wind tunnel triggers earlier transition than in either quiet tunnels or in free flight. Quiet wind tunnels have observed crossflow streaks that appear near the end of the model, and some small turbulent lobes that begin to form at the highest test conditions. As was mentioned previously, there appear to be no disturbances created anywhere on the model from the fiducial markings.

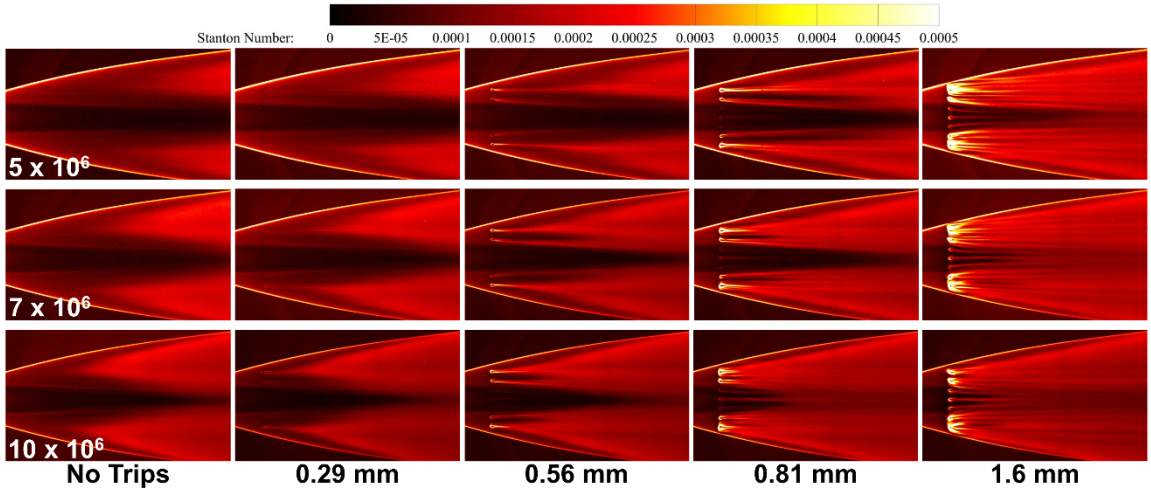

Figure 8. Effect of trip height at three selected unit Reynolds numbers, trips placed at Station 1.

Moving to the second column of images in Fig. 8, the smallest trip height tested, k = 0.29 mm, looks very similar to the no trip case, particularly along the centerline. At all conditions tested, any noticeable effects for the three trips in the center region are indiscernible from the no trip case. The two trips near the outboard region, however, do appear to show faint streaks at Re = 5 million/m, and these streaks grow in intensity as the unit Reynolds number is increased. Compared to the no trip case, a slight movement forward in the transition lobes may be visible as the upper unit Reynolds number limit is reached. Due to the prominence of the turbulent lobes though, any effect of these outboard trips is quickly lost at the higher unit Reynolds numbers as the lobes move upstream closer to the trip locations.

For the next trip height tested, k = 0.56 mm, the results follow a similar trend. Here, the outboard trips all show significant vortices behind the trip that persist into the turbulent lobes at all unit Reynolds numbers. The vortices also now appear to show a slight sweep inboard, an effect of the pressure gradient created due to the concave geometry. While the Re = 5 million/m case is similar to the k = 0.29 mm condition in terms of transition onset behind the trips, at Re = 7 million/m, it now appears that the transition location has moved upstream compared to the smaller trip case, especially for the trip nearer the centerline region. At Re = 10 million/m, transition occurs quite soon behind the outboard trips, and the vortices again get washed out into the turbulent lobes. Along the centerline, faint streaks behind these three trips begin to show up at Re = 7 million/m, although their effect is still somewhat muted. Even at the highest unit Reynolds number of 10 million/m, the streaks are still quite faint and only a slight movement forward of the transition region is seen.

For a trip height of k = 0.81 mm, significant disturbances are now seen on the outboard edges. Here, the trips show a very high heating rate around them, and this heat flux increases as unit Reynolds number is increased, possibly indicating the trips are now near or at the edge of the boundary layer and exposed to the freestream flow. Transition location has also appeared to move significantly upstream compared to the baseline case, and the transition point may in fact be directly behind the trips at higher unit Reynolds numbers. Also noticeable are the streaks, which now persist into the turbulent lobes, and are still somewhat visible even in these higher heating turbulent regions. Finally, on the center region, these trips appear to show distinct vortices even at the lowest unit Reynolds numbers. The vortices

increase in strength and heating, and at Re = 10 million/m, the turbulent region in the center portion of the model has moved significantly upstream from the baseline case, and even the previous trip cases.

For the largest trip height tested, k = 1.6 mm, the outboard trips now show significant disturbances around each trip element. Heating rates at and near the trips are all much higher than in previous cases, again indicating these trips may be out of the boundary layer. Vortices persist well into the turbulent lobes and might even alter the flow in these regions as the vortices churn up the boundary layer and freestream. For all cases, the transition location appears to occur directly behind the outboard trips. The centerline trip vortices clearly show up for all three unit Reynolds numbers, and even at Re = 5 million/m, there is a distinct difference in the heating along the center region. Transition location appears to have moved upstream quite a bit compared to the no trip case. As the unit Reynolds number is increased further, the transition location moves upstream, and higher heating at the trips might indicate these trips are also beginning to approach the edge of the boundary layer.

Many other combinations of trip heights, locations, and planform sizes were tested, and the full results can be found in Ref. 15.

C. Initial Concept for Flight

Following the initial sizing and placement effort, a different approach for tripping was adopted for testing as a potential candidate for the final flight configuration. Here the idea was to see if trip heights could be tailored to the local boundary layer thickness to try to trip the flow at nearly the same Reynolds number regardless of location. At this point in the study, calculations of boundary layer thickness were not available to guide the tailoring, instead the previous results were used to select just the right height for a given location. One set of trip heights and their locations are shown below in Figure 9. All trips were located at 84 mm from the leading edge (Station 1); the 1.6 mm trip was on the centerline, the 0.56 mm trip was 25 mm from the centerline, and the 0.29 mm trip was 37 mm from the centerline. All trips in this configuration have the 1.3 mm square planform size. The centerline trip was chosen to be the largest tape thickness tested previously, k = 1.6 mm. This trip height provided a noticeable wake at even the lowest unit Reynolds numbers, and altered transition location at moderate and high unit Reynolds numbers, without significant local flow disturbances. The smallest trip height, k = 0.29 mm was placed at an outboard location close to the leading edge, while a medium sized trip, k = 0.56 mm, was placed in an intermediate location but transposed to the other side.

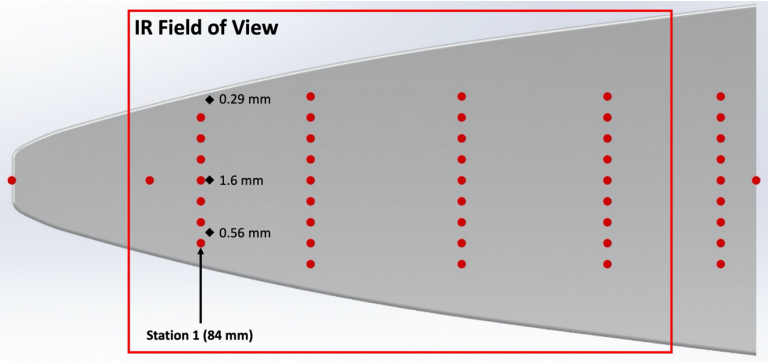

Figure 9. Flight candidate trip heights & locations.

Results for this configuration are shown below in Figure 10 for both the no trip and tripped cases. The lowest unit Reynolds number was 2.5 million/m (the lowest operating range of the M6LT) as this corresponded to the start of the test window expected during flight. At Re = 2.5 million/m, all three trips show vortices directly behind the element, but the vortices from the centerline and medium sized trips quickly disappear into the background heat flux. The outboard (smallest trip) vortices, however, appear to persist considerably farther downstream. As unit Reynolds number is increased to 4 million/m, the vortices increase in strength and heat flux, and all three persist to the end of the field of view. Despite being almost at the leading edge, the smallest outboard trip vortices persist nearly straight back from the trip and do not curve appreciably as was seen when the trip was placed on the leading edge at downstream locations. At unit Reynolds numbers of 7 and 10 million/m, all three trips show localized heating at the trip, and the vortices appear to be causing significant increased heat flux behind them.

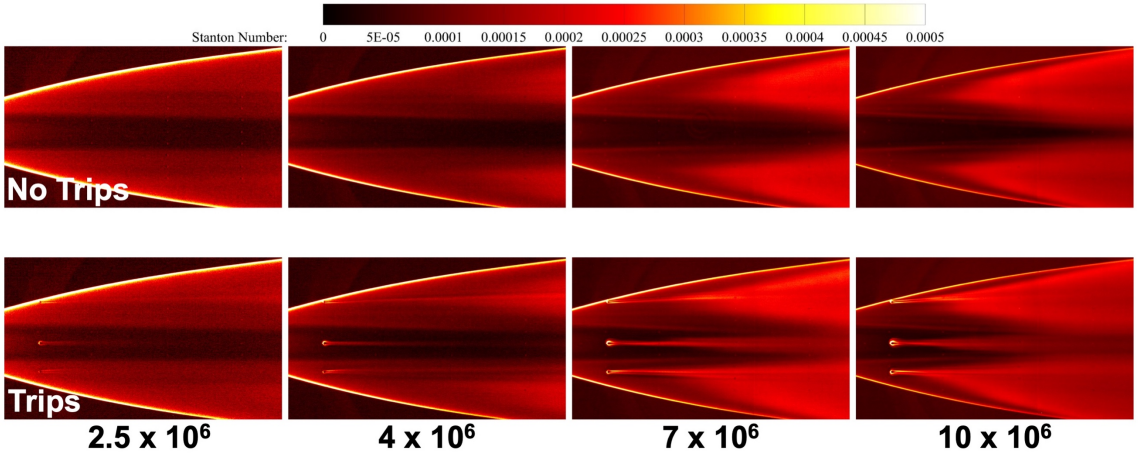

Figure 10. First flight test configuration heat flux results for various unit Reynolds numbers.

As shown in Fig. 10, it was often difficult to decipher when a given trip height and location caused the onset of transition at a significant distance downstream, the so-called "incipient" point, due to the interference provided by the progression of the natural transition lobes. This led to the idea that perhaps the natural lobes could somehow be subtracted from the results. Thus, for this set of testing, care was taken to repeat the measurements without trips so that "background subtraction" could be attempted for visualizing the trips effects. With identical fields of view and measurement parameters, the heat flux from the untripped cases could be subtracted from the heat flux of the tripped cases to show more clearly the effects of the trips themselves. By using this background subtracted method, the qualitative subtracted-heating contour plots of Figure 11 were created. Here the natural transition lobes are removed from the images, so just the effect of the trips remain.

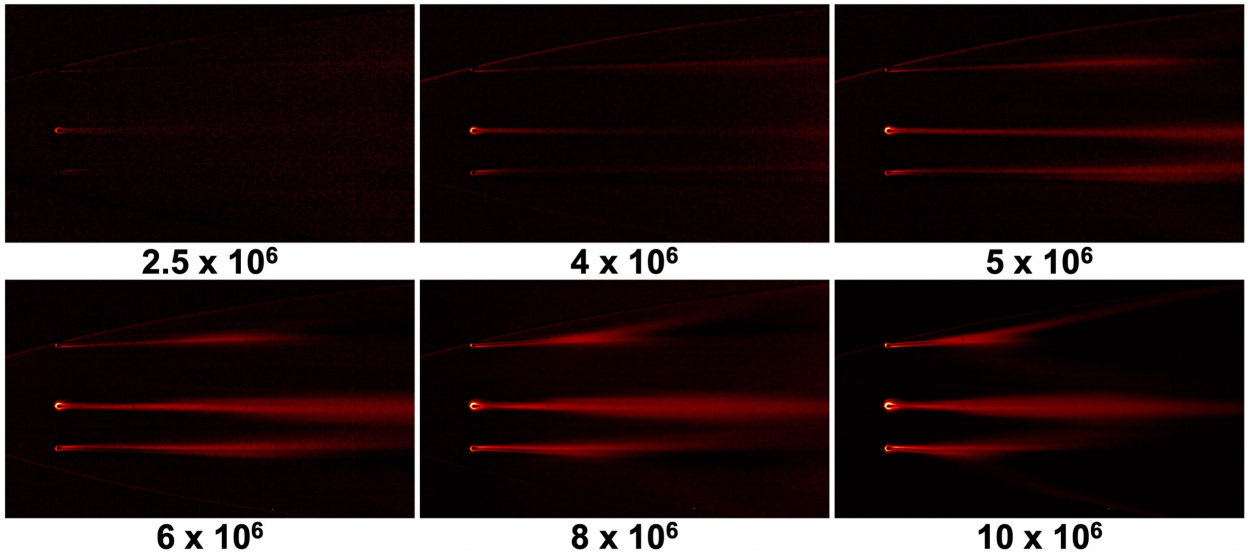

Figure 11. Initial flight configuration shown with background subtracted for various unit Reynolds numbers.

Starting with the centerline trip, at the lowest unit Reynolds numbers of 2.5 million/m, a wake is observed behind the trip, but does dissipate quickly and blends into the background heat flux before reaching the end of the model. At Re = 4 million/m, the wake now appears to very weakly persist to the end of the field of view. Finally, at Re = 5 million/m, the trip vortices are strong, persist to the end of the field of view, and there appears to even be some spreading of the turbulent wedge near the end of the field of view. This spreading increases as unit Reynolds number is increased, and the intensity of the vortices grows stronger directly behind the trip. At the highest unit Reynolds numbers of 8 – 10 million/m, the spreading appears to have reached a maximum, and heat flux at the end of the field of view appears to decrease as the natural transition lobes become more prominent.

For the medium sized outboard trip, like the centerline trip, vortices appear to form from Re = 2.5 – 4 million/m, but they are weak and mostly unable to overcome the natural heating of the boundary layer. Following the trend of the centerline trip, some spreading of the turbulent wedge begins to appear at Re = 5 million/m, but above this unit Reynolds number, much of the wake of this trip gets lost in the natural transition lobes.

The smallest outboard trip shows a noticeably different pattern than either of the preceding two trips. Here, even at the lowest unit Reynolds number, the vortices can be seen faintly reaching the edge of the field of view, and at Re = 4 – 5 million/m, these vortices stand out from the background. The vortices also follow nearly straight paths behind the trip despite the concave geometry and pressure gradients. However, the naturally turbulent lobes begin to obscure the wake of this trip at Re = 5 million/m and above. Some spreading of the turbulent wedge is observed at these higher unit Reynolds numbers until the turbulent lobes nearly overtake the trips at Re = 10 million/m. Interestingly, at Re = 8 million/m and above, there appears to be an offshoot of the turbulent heating from the trip that follows the leading-edge geometry. An exact cause of this heating has not yet been confirmed.

D. Final Flight Configuration

The data presented up to this point (including the full set of results presented in Ref. 15) were used to influence final decisions ahead of the BOLT II project Critical Design Review (where the hardware design was finalized). As will be discussed later, the data did support existing discrete roughness correlations for the onset of transition based on k/δ of 0.7, in agreement with previous results presented in Ref. 17 in support of the Hyper-X program. Without a wider set of data specifically on the BOLT geometry from multiple wind tunnel studies, the decision was made to move forward using the preexisting correlation approach, since it was well supported by the new data. Some additional factors were considered for selecting the final trip locations based largely on the instrumentation budget for the roughness side, which will be discussed in detail in an upcoming section. Long after the review, there was a second opportunity to test within the USAFA M6LT, and therefore the actual final flight configuration was also examined. The new fiducial layout used for the second entry, along with the trips studied are presented in Figure 12. For this final set of experiments, the trips were applied at the locations below, and the fiducial marking layout was changed as well. The 0.81 mm trip is on the centerline again, and both 0.29 mm trips are 49.5 mm from the centerline and symmetric about it. This symmetric configuration was chosen for more redundancy in collected data.

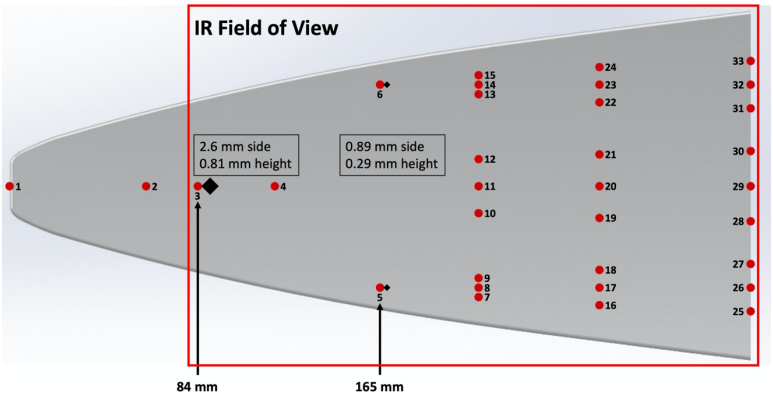

Figure 12. Final trip location and fiducial layout.

As before, testing was conducted both with and without trips using identical setups, and unit Reynolds numbers from 2.5 to 10 million/m were investigated. The background subtracted images from this configuration are shown in Fig. 13. At the lowest unit Reynolds number of 2.5 million/m, faint streaks are barely visible directly behind all three trips, but these streaks are quickly swallowed by the background heating on the surface. For the outboard trips, there appears to be some evidence of the turbulent wedges developing and showing at the very back of the model near the trailing edge, although these wedges show very low heating augmentation and probably little to no actual boundary layer transition. As the unit Reynolds number is increased to 4 million/m, the streaks are more prominent behind the trips. The centerline trip still shows very fast dissipation of the vortices, with little to no change in the heating after the midpoint of the model. The outboard trips show clearer vortices developing behind them, and a turbulent wedge behind each trip is clearly visible from the midpoint of the model as it grows and spreads toward the trailing edge, indicating the presence of turbulent flow created by the trips.

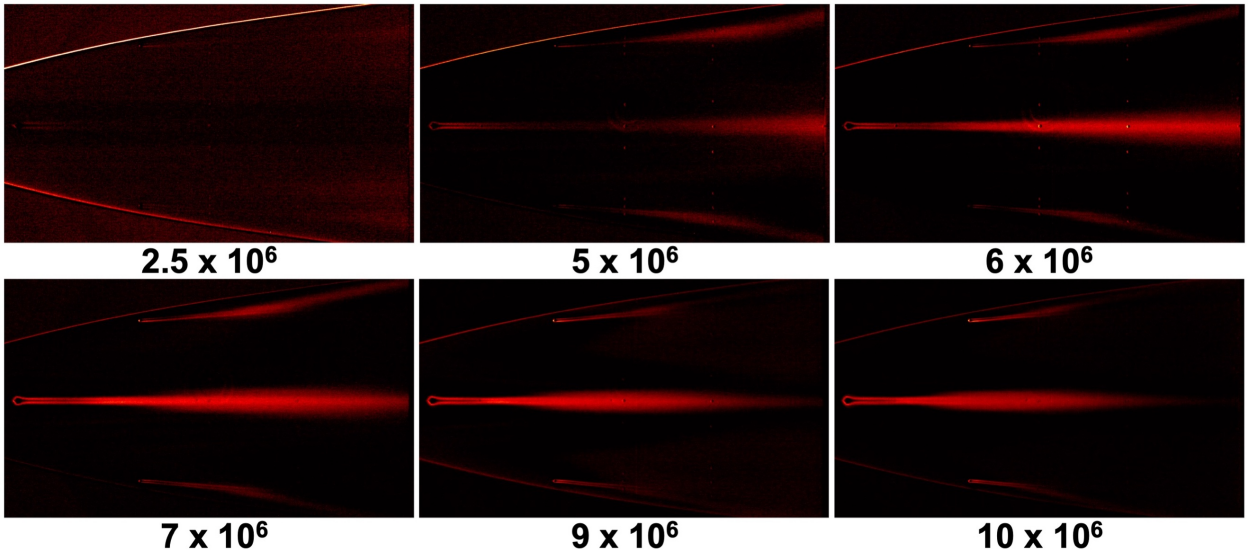

Figure 13. Final flight test configuration background subtracted results for various unit Reynolds numbers.

At unit Reynolds numbers of 5 million/m and above, the centerline trip finally appears to influence the baseline flow. Streaks are clearly visible directly behind the trip, and a turbulent wedge appears, grows, and spreads behind the trip. The turbulent wedge is most prominent and widest at the trailing edge at a unit Reynolds number of 6 million/m. At Re = 7 million/m and above, the turbulent wedge begins to contract near the trailing edge as the outboard lobes increase the baseline heating near the centerline, and at Re = 9 million/m and above, the turbulent streak near the trailing edge begins to disappear as the centerline boundary layer becomes naturally turbulent, thereby diminishing the effect of the trip farther downstream of its application.

For the outboard trips, the turbulent streaks behind each trip continue to grow and spread as they follow the model leading edge geometry for unit Reynolds numbers of 5 million/m and above. The streaks appear to increase in heating intensity while their paths and influence remain relatively unchanged until Re = 9 million/m. At this unit Reynolds number, the turbulent lobes increase the background heating and the streaks from the outboard trips begin to disappear near the end of the model. At the two highest unit Reynolds numbers, the streaks do not appear to persist past roughly the midpoint of the model as the natural transition lobes dominate these regions in the wind tunnel flow. As mentioned previously, these natural lobes are not expected to appear at these conditions in flight due to the quiescent nature of the incoming flow, and therefore the turbulent streaks from these trips should continue to develop.

V. Computational Analysis and Extraction of BL Properties

A. Methodology

Computational results for the BOLT flowfield were needed both to support the USAFA wind tunnel experiments and extrapolate the results to flight conditions. Two Computational Fluid Dynamics (CFD) solvers were used in order to decrease turn-around time: DPLR[19] and US3D.[20] DPLR solutions were computed using a 3rd-order MUSCL Steger-Warming scheme for the inviscid fluxes and 2nd-order central differences for the viscous fluxes. The solutions calculated in US3D used a 2nd-order Modified Steger-Warming scheme and a central deferred-correction approach for the inviscid and viscous fluxes, respectively. All cases were run assuming laminar flow and using a structured grid with about 60 million cells (unless otherwise noted). Boundary-layer height, δ, was based on the wall-normal height where the flow regained 99.5% of the total enthalpy of the freestream.

Three sets of data were produced. Table 3 shows eight flight conditions that were chosen within the experimental window. The flight cases were computed with a 400 K isothermal wall, which is consistent with the surface temperatures expected during the BOLT flight.[21] These solutions were used to both track the direction of expected turbulent wedges and to get estimates for the boundary-layer heights near potential target conditions. Next, a subset of wind tunnel conditions was calculated, detailed in Table 4. This was on a 33% scale model with a constant wall temperature of 300 K. Finally, two cases were chosen to prove convergence of the boundary-layer heights that were being provided. The Flight Verification cases in Table 5 were chosen from an ongoing analysis being done with a BOLT trajectory point (not BOLT II), and the Wind Tunnel Verification cases were based on cases from BOLT wind

tunnel experiments at Purdue University. These two sets of conditions are similar enough to the BOLT II flight and USAFA wind-tunnel conditions that grid-convergence properties should apply to the conditions in Tables 3 and 4.

Table 3: Flight conditions used to study the properties of the boundary layer on BOLT II.

Case	Mach	Unit Reynolds [1/m]	Solver
Ascent 1	5.3	18.21 x 10^6	US3D
Ascent 2	6.1	11.93 x 10^6	US3D
Ascent 3	5.8	4.13 x 10^6	US3D
Ascent 4	5.5	1.55 x 10^6	DPLR
Descent 1	5.3	1.54 x 10^6	DPLR
Descent 2	5.5	5.09 x 10^6	DPLR
Descent 3	5.6	8.82 x 10^6	DPLR
Descent 4	5.6	15.26 x 10^6	US3D

Table 4: Simulated conditions to match USAFA wind tunnel experiments.

Case	Mach	Unit Reynolds [1/m]	Reynolds	Solver
Wind Tunnel 1	5.9	2.5 x 10^6	0.83 x 10^6	DPLR
Wind Tunnel 2	5.9	4.0 x 10^6	1.3 x 10^6	DPLR
Wind Tunnel 3	5.9	10.0 x 10^6	3.3 x 10^6	DPLR

Table 5: Conditions used in the grid convergence study.

Case	Grid Size [cells]	Mach	Unit Reynolds [1/m]	Reynolds	Wall Temp [K]	Solver
Flight 1	50 x 10^6	5.2	11.52 x 10^6	11.52 x 10^6	400.	DPLR
Flight 2	100 x 10^6	5.2	11.52 x 10^6	11.52 x 10^6	400.	DPLR
Flight 3	200 x 10^6	5.2	11.52 x 10^6	11.52 x 10^6	400.	DPLR
Flight 4	400 x 10^6	5.2	11.52 x 10^6	11.52 x 10^6	400.	DPLR
Wind Tunnel 1	50 x 10^6	6.0	9.88 x 10^6	3.29 x 10^6	300.	DPLR
Wind Tunnel 2	100 x 10^6	6.0	9.88 x 10^6	3.29 x 10^6	300.	DPLR
Wind Tunnel 3	200 x 10^6	6.0	9.88 x 10^6	3.29 x 10^6	300.	DPLR

B. Results

After exploratory experiments were completed in the USAFA tunnel, two specific regions of the flow were chosen to trip. One region was the centerline of BOLT II, which has a thick boundary layer surrounded by stationary vortices. The other region was near the leading edge of the vehicle where the boundary layer is much thinner. For correlation purposes, boundary-layer heights were extracted in these regions at each of the flight conditions listed in Table 3. These heights can be seen in Fig. 14. The various trajectory points all have very similar Mach numbers, resulting in the boundary-layer heights scaling very well with $Re^{-1/2}$.

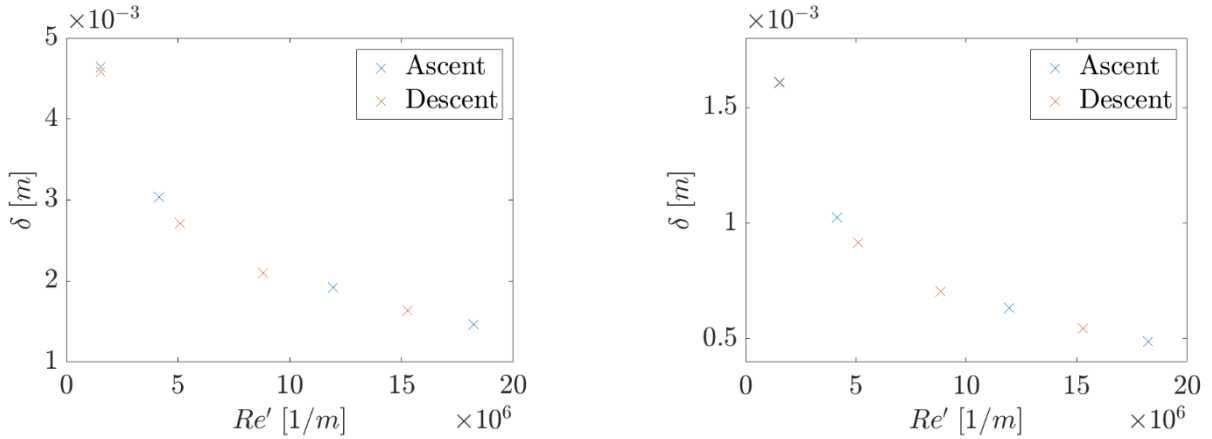

a) Centerline trip: X = 0.254 m, Z = 0.0 m b) Leading edge trip: X = 0.5 m, Z = ± 0.15 m

Figure 14. Boundary-layer heights for the trip locations at each flight trajectory point in Table 3.

Heights were also calculated at the wind-tunnel-trip location so that the boundary-layer parameters could be estimated at conditions where transition was observed in experiments. Additionally, the streamline directions were sought to help place sensors downstream of the trips. As shown in the comparison of Fig. 15, with the infrared image (Fig. 15a) providing evidence of the wake behind three trips and calculated streamlines at the edge of the boundary layer (Fig. 15b), the measured streaks reflect the computations. Not unexpectedly, the flow behind the trip on centerline closely matches the centerline streamlines. Additionally, the trip near the leading edge does provide for a wake that follows a slightly outboard direction, while the midway trip has a wake that goes slightly inboard, both in agreement with the computations. Thus, streamline calculations at flight conditions based on the boundary layer edge were used to locate the sensor array for flight (as will be shown in a subsequent section). The computed streamlines were also a factor in choosing to trip the leading-edge region as opposed to the midspan location. The wedge from the leading-edge trip follows a more predictable path over the entire experimental window because it does not cross the natural stationary features that set up toward the center of BOLT II. Any trip placed at a midspan location would have its transition characteristics marred by these vortices, making interpretation of the flight experiment more difficult.

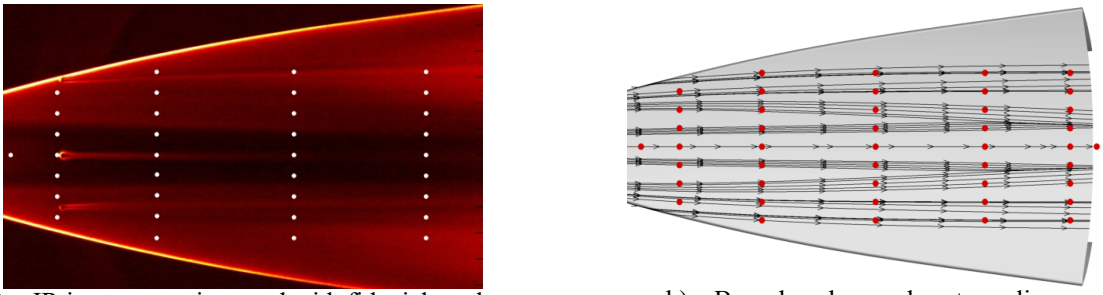

a) IR image superimposed with fiducial marks b) Boundary-layer edge streamlines

Figure 15. Comparison of streaks behind trips from wind tunnel to inviscid streamlines calculated at same condition.

Using the wind tunnel boundary layer calculations to examine various parametric approaches did not yield an obvious correlation of results for moving forward. Given more time, other wind tunnel results, including data from both conventional and quiet facilities, would have been sought. However, the flight project required decisions much sooner than would be allowed by seeking additional wind tunnel entries. The closest thing to a correlation that was observed in the present dataset was a simple threshold based on scaling the trip height to boundary layer thickness (k/δ). This approach was similar to that used for Hyper-X for sizing wind tunnel derived trips results for flight and subsequently shown through flight data analysis to have worked.[Error! Bookmark not defined.] Going back to the data presented in Fig. 11, one can observe that the wakes generated by the three trips all appear to become more prominent, and thus are interpreted as then being "incipient," at around Re=5 million/m. Based on the boundary layer thickness spanning the model at Station 1, and if all three are truly incipient at that Re, then the resulting k/δ associated with each trip would be roughly 0.7. Perhaps, the lack of granularity in trips heights and/or Re, along with the interference coming from the natural transition lobes under conventional wind tunnel conditions, contributed to the project's inability to identify a true correlation from the data in hand. Time permitting, it is recommended that additional wind tunnel studies are pursued to further investigate tripping correlations on the BOLT geometry, hopefully in a variety of facilities.

C. Verification of CFD Results

As mentioned in the Methodology section, grids with 60 million cells were used for all the flight and wind-tunnel calculations. In order to prove that these grids were accurate enough for this study, a grid-convergence study was performed at both a flight and wind-tunnel condition. In Reference 22, these two conditions are studied in detail with respect to the convergence of Stanton number and axial-velocity contours in the boundary layer. Here, the parameter of interest is the boundary-layer height. Figure 16 shows what locations were used when extracting this data. Green circles correspond to the flight-vehicle trip locations, while the blue crosses are where most of the wind-tunnel trips were placed. Relative error is calculated for the less-resolved solutions as shown in Equation 1. For the flight cases, shown in Figures 17a and 17b, the reference value is the boundary-layer height calculated from the 400 million cell solution. For the wind tunnel cases, the solution was deemed to be satisfactorily converged at 200 million cells, so this solution is used for the reference δ. From the results in Figures 17, the boundary-layer height for the 50 million cell solution is always within 0.5% of the height calculated with a more-resolved grid. Further, the error reduction is monotonic as the number of grid cells is increased, so it is unlikely that any unexpected changes would appear if the

higher grid counts were used. This gives confidence that the grids used for this study were satisfactory and that the solutions are grid-converged relative to the boundary-layer heights at the trip locations.

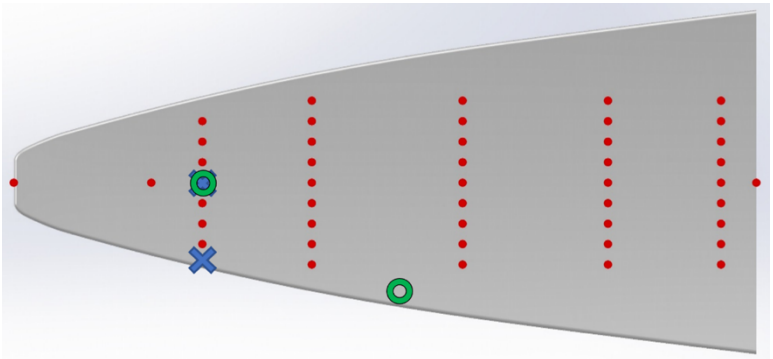

Figure 16. Locations used for grid-convergence study of boundary-layer thickness.
Green circles for flight cases. Blue crosses for wind tunnel cases.

$$Relative\ error = \frac{|Current\ resolution - Maximum\ resolution|}{Maximum\ resolution} \quad (1)$$

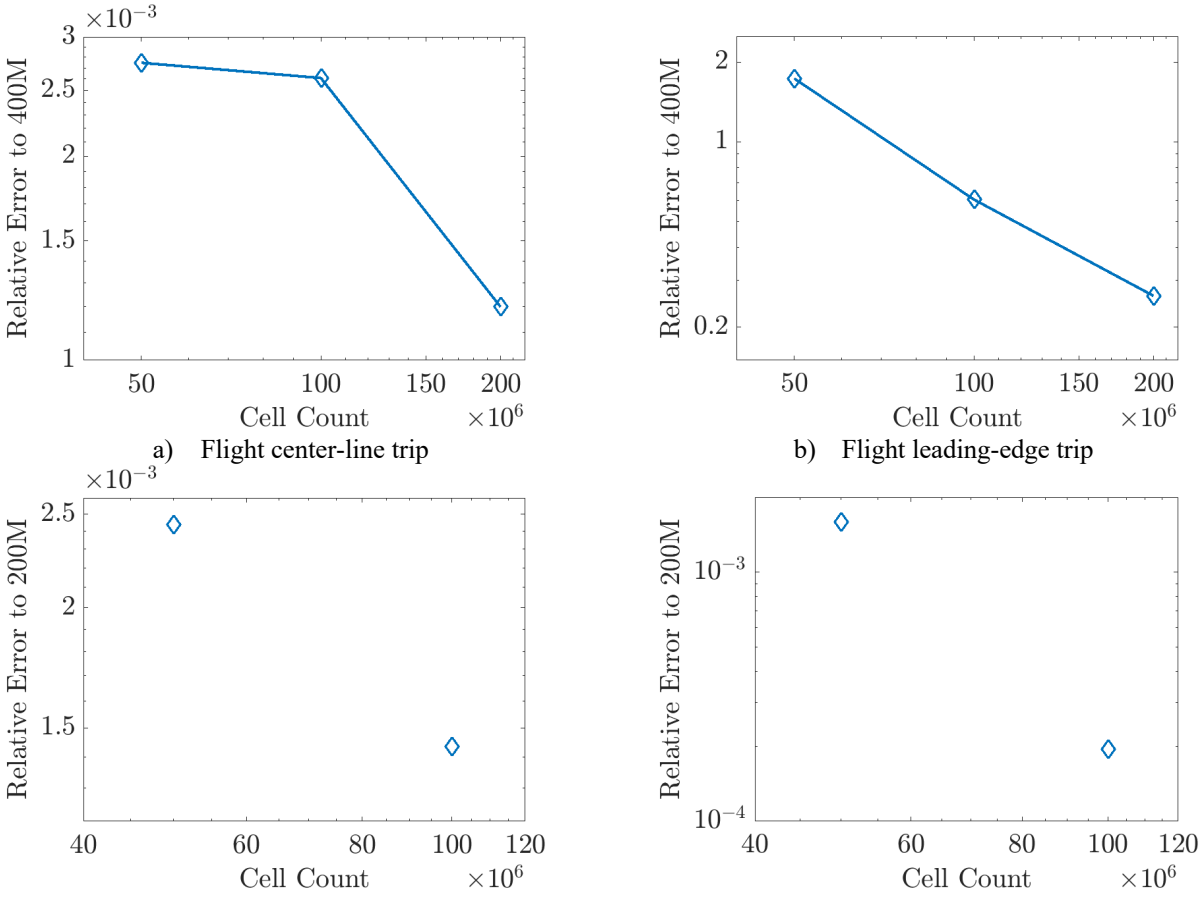

a) Flight center-line trip
b) Flight leading-edge trip
c) Wind-tunnel center-line trip
d) Wind-tunnel leading-edge trip

Figure 17. Relative error of the boundary-layer height at various trip locations.

VI. Finalization of the trips for Flight

The prior sections describe some of the key inputs to down selecting to a final set of trips for flight, mainly the experimental results obtained in the USAFA M6LT and the boundary layer calculations and properties used to help

correlate the experimental results and then scale the trips to flight. However, an equally important driver in the final determination of a plan for tripping in flight was based on the number of available sensors for the roughness side experiment. As was done previously with the first BOLT campaign, the lion's share of the instrumentation budget was dedicated to the primary objective of the science mission, the smooth side measurements. For BOLT II, after careful consideration of the smooth side instrumentation requirements, the roughness side was allocated 38 surface thermocouples (Medtherms), 4 pressure measurements (Honeywells) dedicated to FADS (for determination of alpha/beta variations), 12 high-frequency pressure measurements (7 PCB's and 5 Kulites®), 12 heat-flux sensors (Thermogage), and 12 thin-film sensors (provided by CUBRC). Based primarily on the number of surface thermocouples, an early decision was to only target three distinct and separate trips for the roughness side experiment. The thermocouples would be spaced axially downstream of each trip to track the onset and movement of the transition behavior during flight. Also, a few of the thermocouples would be used to measure the local surface temperatures on and around the trips. The pressure, heat flux, and thin-film gauges are intended to compliment both the roughness side thermocouples (specifically to map the movement of the developing turbulent wedges using spanwise groupings), as well as for comparison to similar measurements on the smooth side.

Having conceptually determined that 3 was the right number of trips, the next question was where to locate them. Placing a trip on the vehicle centerline seemed an obvious choice, and using the location that had been heavily tested in the tunnel (Station 1) was quickly agreed to by the team. This set the location for the first trip at X=0.254m and Z=0.0m. The other two locations had to be somewhere outside the zone of influence of the centerline trip and corresponding sensor array. At first, outboard locations in line with the centerline trip (i.e., all on Station 1) were considered. But when devising the downstream sensor layout for these outboard locations, including the spanwise sensor arrays (whose function was to map the spreading angle once the trip forces a turbulent wedge to move significantly forward), it then became obvious that all the sensors would be clustered too close to each other, and that cross contamination from one trip might interfere with the intended measurements from the other trip. For this reason, it was decided to place the two additional trips closer to both swept leading edges of BOLT II, but then slide them further down the body to allow for better separation between the three sensor groupings, while still maintaining some running length behind these outboard trips. With this decision, the locations for the final two trips were set at X=0.5m and ±Z=0.15m. The final consideration regarding these outboard locations was to make them mirror images of each other, in hopes of providing "redundancy" data. The centerline trip is expected to be somewhat insensitive to small alpha/beta variations during flight as the incoming flow to the trip is largely planar. On the other hand, the flow in front of trips near the leading edges should be crossflow dominated and thus these trips are expected to be more sensitive to small alpha/beta changes, and for this reason making them the same allows for comparison of data from each side as flight maneuvers happen. One final note regarding these stated locations is that they represent the center of each trip, and not the leading corner of the trip as was done during the tunnel testing.

Next up was to determine the size of the trips (both height and width) to place at these chosen locations. As mentioned previously, once the computed boundary layer properties were used to examine correlations from the new experimental data, a consistent k/δ value on the order of 0.7 seemed an excellent threshold for when onset would occur downstream of the trips. As it turned out, this value was in agreement with a previous correlation of tripping that had been established for the Hyper-X flight vehicle (Ref. 17), which was also a sharp, slender configuration that flew at a similar Mach number and Reynolds numbers to the present case. With consideration of the previous flight trajectory points identified in Table 4 and the change in boundary layer thickness expressed in Fig. 12, one final tweak was implemented in deciding how to size the trips. There was concern based on the wind tunnel data that if the trips were sized based on a trajectory point with a higher Reynolds number, then the chance of the natural transition lobes to present themselves in flight, and interfere with the measurements of onset behind the trips, became greater. Thus, an intermediate descent point was selected between D1 and D2, what the team designated as D1.5 with a unit Reynolds number of 2.5 million/m. The boundary layer thickness at both the centerline and leading-edge locations for the D1.5 case was used to finalize the trip height. For the centerline location, the boundary layer thickness at D1.5 was calculated to be 0.00375m. Thus the trip height became 0.002525 m, based on the k/δ of 0.7. Similarly, the calculated boundary layer thickness at the leading-edge location was 0.000129 m, which provides for a trip height of 0.000903 m. The final input was to select an aspect ratio for the trip width to trip height (b/k) of 3. Based on the analysis detailed in Ref. 23 where it was suggested that the aspect ratio of the trips could influence the resulting onset data, the decision here was to be consistent with the same aspect ratio for all three trips. This results in the centerline trip being 0.007875 m wide and the leading-edge trips being 0.002709 m.

Figure 18 provides a sketch of the trip locations and supporting instrumentation layout for the BOLT II Roughness Side experiment. The trips were designed and built as part of machined structure, to simplify the conduction path into the vehicle as a heat sink. As was described above, three separate sensor groupings are shown that were placed with the intent to measure the onset and movement of transition using surface thermocouples. Two of the groupings (shown

in Fig. 18 on centerline and lower leading edge) were augmented with spanwise thermocouples, heat-flux, and thin film sensors for measuring the spreading angle from the developing turbulent wedges. Pressure gauges were located both in front of and downstream of the trips. Some of the sensor locations on roughness side were specifically chosen as potential replicate measurement for comparison against the smooth side of the vehicle.

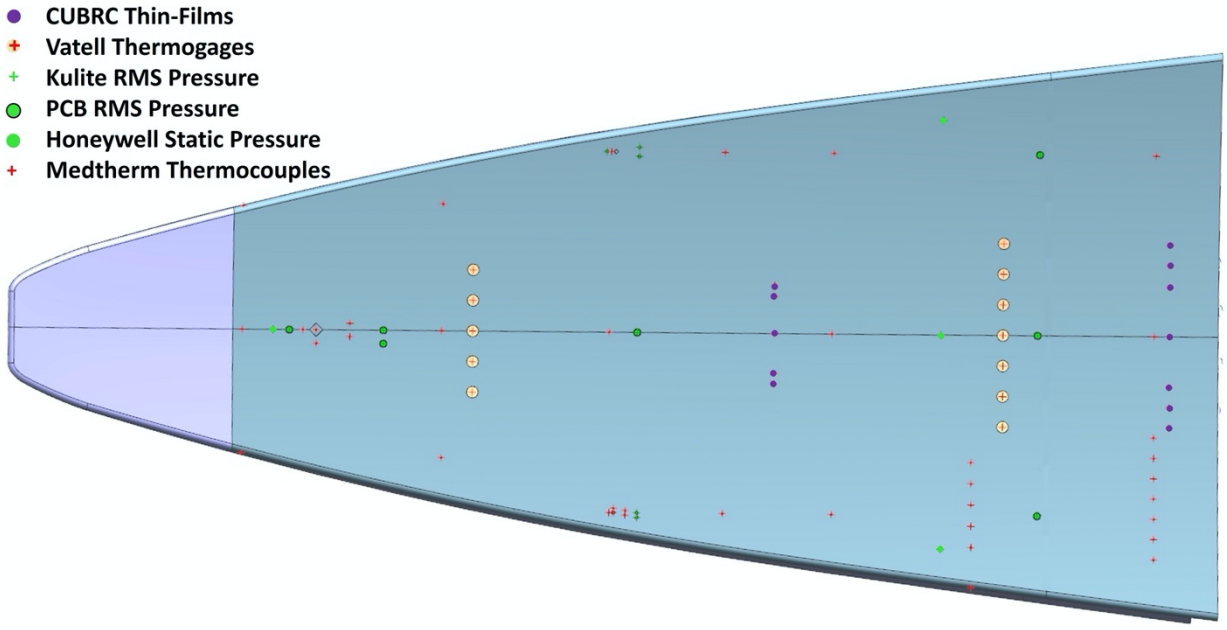

Figure 18. Trip locations and sensor layout for the BOLT II Roughness Side experiment.

VII. Structural-Thermal Analysis of final trips

A finite element analysis of the integral trip design was conducted to ensure trip integrity throughout the flight. The initial baseline convective heating analysis was based on a smooth-wall fully turbulent conjugate heat transfer results from CFD++ computational fluid dynamic calculations. The conjugate heat transfer results included a 20% increase in convective heating coefficients to add in conservatism for trajectory variability and other factors. The trip finite element analysis focused on the region near the trips only based on on these smooth-wall CFD solutions with augmentation factors to account for the trip. Augmentation factors were applied to estimate trip surface temperatures and structural integrity throughout flight. Table 6 shows cold-wall convective heating augmentation factors for various trip form factors in a laminar boundary layer. This table of results were derived from preliminary calculations, done as part of the present investigation, for a series of aspect ratios corresponding to the previously mentioned HyBoLT geometry and flow conditions. Turbulent boundary layer augmentation rates would be similar and hot-wall augmentation factors would be reduced further. A conservative 10x augmentation factor (for the b/k=3 form factor) was applied to all five faces of the trips for this analysis. Note that while k/δ does vary throughout the trajectory, the points at which it would exceed 0.75 are early in flight when the heating is quite low and very late when it doesn't matter anymore.

Table 6. Convective Heating Augmentation Factors.

b/k	k/δ	Stanton Number Ratio to smooth wall value
3	0.75	8.9
2	0.75	10.3
1.41	0.75	11.8
0.75	0.75	13.7

Since the trips are machined directly into the exterior surface, the trips are conduction cooled and shed heat to the body. The trips are small, and this conduction affected zone is very localized extending only one trip width away in both lateral and depth directions, see Fig. 19. Instrumentation in the immediate vicinity of the trip could be affected by this higher heating, but this effect would be small and there is no structural impact. The worst case predicted

temperature for either trip for this extreme case was under 1600°F. Stainless steel 410 has a melting point of nearly 2800°F and only begins to see oxidation effects (where a protective chromium-oxide film forms on the surface) at temperatures between 1300-1500°F. Scaling and spalling also will not be an issue since that does not occur until higher temperatures, at greater than 1,800°F. Lastly, it should be noted that the maximum recovery temperatures through the nominal trajectory never exceeds the melting temperature of stainless 410.

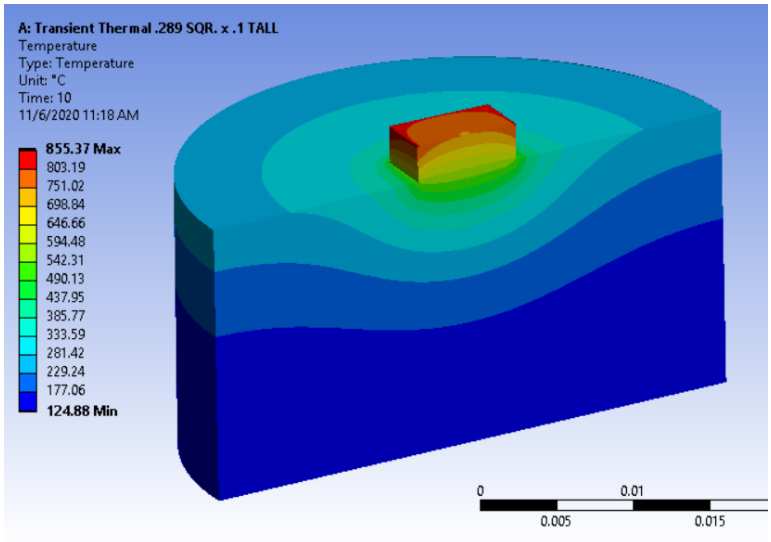

Figure 19. Finite Element Analysis of Centerline Trip.

Knowing that the trip surface might at worst see "oxidation" temperatures for only a few seconds during flight, no thermal or structural concerns seem warranted. Note that the centerline and port trip will have a surface thermocouple to monitor the temperature throughout flight. Pictures of the as-built trips and some of the instrumentation are shown below in Fig. 20. Figures 20a and 20b were taken after machining, but prior to installation of any sensors (three holes for surface thermocouples are shown in Fig. 20b). Also, as can be seen in Fig 20b, the bottom radius and top corners of the trips were left as sharp as possible. Molds and final inspection measurements and photos will be taken after instrumentation is completed, again after wind-tunnel testing, and again before flight after environmental testing is completed. Figures 20c-e show close-ups of the trips after sensor installation was completed. A few words about the instrumentation shown in Fig. 20. The Medtherm's provide both a front-face and back-face measurement and were installed such that the back-face thermocouple junction was aligned with the inner wall surface, and then the front-face junction was sanded flush with the vehicle exterior surface. The process of sanding the thermocouple flush to the surface, specifically to form the surface junction, tends to blend them with the surface, and can make them hard to see in some cases (for instance, see Fig. 20d). All gauges (with the exception of the PCBs) are intended to be installed flush to the surface, but due to the relatively low vehicle surface curvature, small recesses (less than 0.025 mm) can occur (for instance, see Fig. 20c). In Fig. 20c, two Kulites® with "B" screens are seen in the photo (also three are shown in Fig. 20e) The PCBs were recessed 0.25 mm and then covered with a thin layer of RTV to "fill the recess" for added protection against sudden changes in temperature. The red RTV is seen in Fig. 20d. Frequency response in the range of interest for these gauges will not be affected by the thin coating. RTV is rated to 533 K and will slowly ablate at temperatures above 570 K, but surface temperatures in general should not exceed that temperature. Some minor erosion of this thermal protection layer should not adversely affect the other surface measurements. Lastly, a pressure tap associated with a Honeywell static pressure measurement is seen ahead of the trip in Fig. 20d.

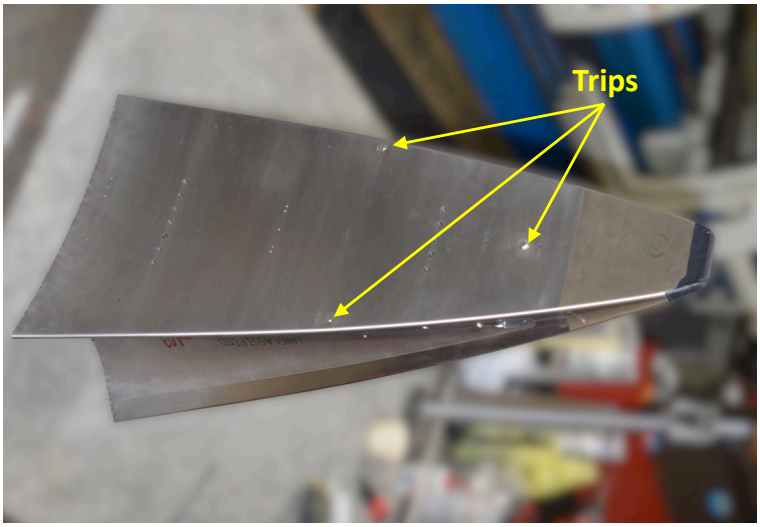

a. Pre-Instrumentation Assembly

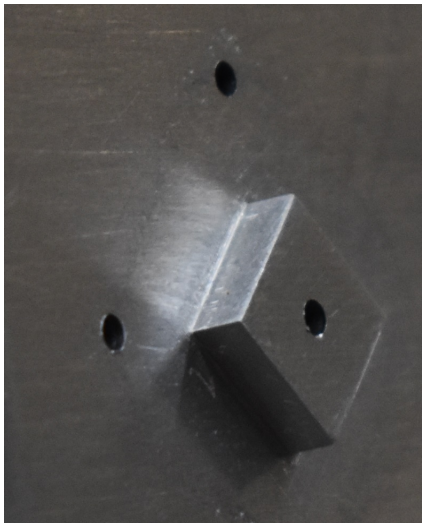

b. Pre-Instrumentation Centerline Close-up

c. Port Trip

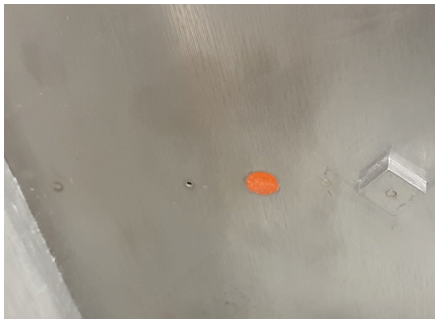

d. Centerline trip

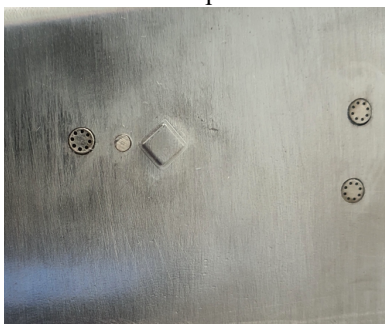

e. Starboard Trip

Figure 20. Various photographs of the as-built trips and instrumentation.

VIII. Summary

The present paper provides a review of the decisions made in developing the roughness side experiment for the BOLT II flight. A combined experimental and computational effort was undertaken to develop the roughness experimental plans for this mission. A wind tunnel test campaign took place in the USAFA M6LT using a 33% scale model, which examined a number of different trip locations, heights and planform sizes. Computational mean flow solutions were computed at wind tunnel conditions (to investigate tripping correlations from the experimental results) and at flight conditions using two codes: DPLR and US3D. While various attempts at correlating the wind tunnel results did not identify a clear winner, a simple scaling of the trip height to boundary layer thickness ($k/\delta = 0.7$) was used to size the trips for flight conditions. This same approach had been used successfully with the Hyper-X program many years before. Three separate trips were selected with one being on the vehicle centerline and the other two being near the swept leading edges and made identical (to allow for post-flight analysis of alpha/beta variations). Based on the available sensor allocation for the roughness side, groupings of thermocouples, pressure sensors, thin-film gauges, and heat-flux gauges were located with the intent to be able to measure the onset of transition behind the trips, as well as the growth of the turbulent wedge. Finally, a finite element analysis of an integral trip design was completed to insure that trips were robust enough to withstand the planned flight trajectory.

Acknowledgments

NASA's contribution to the BOLT and BOLT II projects comes from the Hypersonic Technologies Project, Advanced Air Vehicles Program, Aeronautics Research Mission Directorate. The DoD HPCMP Hypersonic Vehicle Simulation Institute provided support to the USAFA to conduct the wind tunnel testing. The computational work on the BOLT and BOLT-II geometries is supported by AFRL/AFOSR under grant numbers FA9550-18-1-0010 and FA9550-19-1-0154, respectively, with program officers Drs. Ivett Leyva and Sarah Popkin. The authors are grateful to Pointwise and NASA for providing the Pointwise meshing program and the DPLR CFD code, respectively. The

authors also acknowledge the Texas Advanced Computing Center (TACC) at The University of Texas at Austin for providing high performance computing (HPC) and storage resources that have contributed to the research results reported within this paper. In addition, portions of this research were conducted with the advanced computing resources provided by Texas A&M High Performance Research Computing. CUBRC's support comes from the same two grants mentioned above. Support to the University of Arizona was provided by AFOSR, with Sarah Popkin as the Program Manger.

The authors would also like to thank Bryan Morreale and Rodney Bowersox for providing the US3D solutions to support the computational analysis and Christoph Hader for CFD roughness calculations.

References

[1] Dolvin, D., J., "Hypersonic International Flight Research and Experimentation (HIFiRE) Fundamental Sciences and Technology Development Strategy," AIAA Paper 2008-2581, Apr. 2008.
[2] Leyva, I. A., and Cummings, R., "Introduction to the Special Section on the Boundary Layer Transition (BOLT) Flight Experiment," Journal of Spacecraft and Rockets 2021 58:1, pp. 4-5. [doi: 10.2514/1.A34872]
[3] Wheaton, B. M., Araya, D. B., Berridge, D. C., McKiernan, G., Bitter, N., "Initial Results from the BOLT Flight Experiment," AIAA Paper intended for SciTech 2022.
[4] McKiernan, G., Chynoweth, B., Schneider, S., Berridge, D. C., Wheaton, B. M., "Boundary Layer Transition Preflight Experiments in a Mach-6 Quiet Tunnel," Journal of Spacecraft and Rockets 2021 58:1, pp. 54-66. [doi: 10.2514/1.A34772]
[5] Moyes, A. J., and Reed, H. L., "Preflight Boundary-Layer Stability Analysis of BOLT Geometry," Journal of Spacecraft and Rockets 2021 58:1, pp. 78-89. [doi: 10.2514/1.A34792]
[6] Thome, J., Knutson, A., and Candler, G., "Boundary Layer Instabilities on BOLT Subscale Geometry," AIAA Paper 2019-0092, Jan 2019.
[7] Knutson, A. L., Thome, J. S., and Candler, G. V., "Numerical Simulation of Instabilities in the Boundary-Layer Transition Experiment Flowfield," Journal of Spacecraft and Rockets 2021 58:1, pp. 90-99. [doi: 10.2514/1.A34599]
[8] Berry, S., Wheaton, B., and Chynoweth, B., "Secondary Side Considerations for BOLT Flight Experiment," Journal of Spacecraft and Rockets 2021 58:1, pp. 18-25. [doi: 10.2514/1.A34778]
[9] Choudhari, M., Li, F., and Paredes, P., "A Computational Analysis of Boundary Layer Instability over the BOLT Configuration," AIAA Paper 2021-1207, Jan 2021.
[10] Li, F., Choudhari, M., and Paredes, P., "Transition Analysis for Isolated Trips on BOLT II Wind Tunnel and Flight Configurations," AIAA Paper 2021-2905, Aug. 2021.
[11] Popkin, S., Adamczak, D., Morreale, B.J., Swinny, E., Kostak, H., Bowersox, R. D., White, E. B., Dufrene, A., and Wadhams, T., "Science Mission Experiments in Support of the Boundary Layer Turbulence (BOLT II) Flight Test in Memory of Dr. Michael Holden," AIAA Paper intended for SciTech 2022.
[12] Berry, S., King, R., Kegerise, M., Wood, W., McGinley, C., Berger, K., Anderson, B., "Orbiter Boundary Layer Transition Prediction Tool Enhancements," AIAA-2010-0246, Jan. 2010
[13] Berry, S.; Chen, F.; Wilder, M.; and Reda, D.; "Boundary Layer Transition Experiments in Support of the Hypersonics Program," AIAA-2007-4266, Jun. 2007
[14] Cummings, R.M., "Hypersonic Ludwieg Tube Design and Future Usage at the US Air Force Academy," AIAA Paper 2012-0734, Jan. 2012. [doi: 10.2514/6.2012-734]
[15] Semper, M., and Cummings, R., "Hypersonic Trip Development for BOLT-II," AIAA Paper intended for SciTech 2022.
[16] Ishiguro, Y., Nagai, H., Asai, K., and Nakakita, K., "Visualization of Hypersonic Compression Corner Flows using Temperature- and Pressure-Sensitive Paints," AIAA Paper 2007-118, January 2007.
[17] Berry, S., Daryabeigi, K., Wurster, K., and Bittner, R., "Boundary Layer Transition on X-43A," Journal of Spacecraft and Rockets, Vol. 47, Num. 6, Nov./Dec. 2010, pp. 922-934. (DOI: 10.2514/1.45889)
[18] Berry, Scott A.; and Horvath, Thomas J.; "Discrete-Roughness Transition for Hypersonic Flight Vehicles," Journal of Spacecraft and Rockets, Vol. 45 No. 2, 2008, pp. 216-227.
[19] Wright, M.J., D. Bose, and G.V. Candler, "A Data-Parallel Line Relaxation Method for the Navier-Stokes Equations," AIAA Journal, Vol. 36, No. 9, 1998, pp. 1603-1609.
[20] Candler, G., Johnson, H., Nompelis, I., Subbareddy, P., Drayna, T., Gidzak, V., and Barhnhardt, M., "Development of the US3D Code for Advanced Compressible and Reacting Flow Simulations," AIAA 2015-1893, Jan. 2015
[21] Wheaton, B. M., Berridge, D. C., Wolf, T. D., Araya, D. B., Stevens, R. T., McGrath, B. E., Kemp, B. L., and Adamczak, D. W., "Final Design of the Boundary Layer Transition (BOLT) Flight Experiment," Journal of Spacecraft and Rockets 2021 58:1, 6-17
[22] Mullen, C. D., and Reed, H. L., "Computational modeling and stability analysis of BOLT hypersonic geometry including off-nominal conditions," Theoretical and Computational Fluid Dynamics, 2021.
[23] Choudhari, M., Li, F., Wu, M., Chang, C., Edwards, J., Kegerise, M., and King, R., "Laminar-Turbulent Transition behind Discrete Roughness Elements in a High-Speed Boundary Layer," AIAA Paper 2010-1575, Presented at the 48th Aerospace Sciences Meeting in Orlando, FL, 2010.